

COLD CO GAS IN THE ENVELOPES OF FU ORIONIS-TYPE YOUNG ERUPTIVE STARS

Á. KÓSPÁL^{1,2}, P. ÁBRAHÁM¹, T. CSENGERI³, TH. HENNING², A. MOÓR¹, R. GÜSTEN³

To appear in ApJ

ABSTRACT

FUors are young stellar objects experiencing large optical outbursts due to highly enhanced accretion from the circumstellar disk onto the star. FUors are often surrounded by massive envelopes, which play a significant role in the outburst mechanism. Conversely, the subsequent eruptions might gradually clear up the obscuring envelope material and drive the protostar on its way to become a disk-only T Tauri star. Here we present an APEX ¹²CO and ¹³CO survey of eight southern and equatorial FUors. We measure the mass of the gaseous material surrounding our targets. We locate the source of the CO emission and derive physical parameters for the envelopes and outflows, where detected. Our results support the evolutionary scenario where FUors represent a transition phase from envelope-surrounded protostars to classical T Tauri stars.

Subject headings: stars: pre-main sequence — stars: variables: T Tauri — stars: circumstellar matter

1. INTRODUCTION

FU Orionis-type objects (FUors) constitute a small group of young stars characterized by large optical-infrared outbursts, attributed to highly enhanced accretion (Hartmann & Kenyon 1996). During these outbursts, accretion rates from the circumstellar disk to the star are in the order of $10^{-4} M_{\odot}/\text{yr}$, three orders of magnitude higher than in quiescence or in normal T Tauri stars. FUors are natural laboratories where not only enhanced accretion but enhanced mass loss can be studied. Most FUors have optical jets, molecular outflows, and optically visible ring-like structures on a 0.1 pc scale that, in some cases, might be connected to expanding shells thrown off during previous outbursts (McMudroch et al. 1993).

Circumstellar envelopes are supposed to play a significant role in the outbursts of FUors, partly by replenishing the disk material after each outburst (Vorobyov & Basu 2006), partly by triggering the eruptions (Bell & Lin 1994). For this reason, envelopes are not static, but evolve with time. Based on the appearance of the $10 \mu\text{m}$ silicate feature, Quanz et al. (2007) defined two categories of FUors: objects showing the feature in absorption are younger, still embedded in a circumstellar envelope; objects showing the silicate band in emission are more evolved, with direct view on the surface layer of the accretion disk. A similar evolutionary sequence was outlined by Green et al. (2006) based on the amount of far-infrared excess. These studies suggest that FUors represent a fundamentally important transition period during early star formation when the embedded protostar clears away its enshrouding envelope to become a Class II T Tauri star (Sandell & Weintraub 2001; Green et al. 2013).

Traditionally, a large part of our knowledge on FUor

envelopes comes from modeling broad-band spectral energy distributions of the dust emission, based on spatially unresolved photometric data mainly at infrared and sub-millimeter wavelengths. The gas component, however, is typically much less studied. With the goal to obtain a general picture of the molecular gas content, we perform a comprehensive and homogeneous survey of all known FUors, by measuring millimeter CO lines using single dish telescopes. In this paper we present observations of the envelopes of eight southern and equatorial FUors, and study the distribution and kinematics of the circumstellar gas, including the characterization of the molecular outflows where detected. Our data reveal the large variety and trends in the envelope structures predicted by the evolutionary models.

2. OBSERVATIONS

Table 1 lists the targets selected for our study from the list of Audard et al. (2014). We used the FLASH⁺ receiver (Klein et al. 2014) at the APEX telescope (Güsten et al. 2006) to measure the ¹²CO(3–2), ¹³CO(3–2), and ¹²CO(4–3) lines towards our targets between 2014 August 23 – 28. APEX is a 12 m diameter millimeter-wave telescope located on the Llano de Chajnantor at 5104 m altitude in the Chilean Atacama desert. FLASH⁺ is a dual-frequency heterodyne receiver, operating simultaneously in the 345 GHz and the 460 GHz atmospheric windows, providing 4 GHz bandwidth in each sideband. The lower frequency channel was tuned to 344.2 GHz in USB to cover the ¹³CO(3–2) at 330.588 GHz, and the ¹²CO(3–2) at 345.796 GHz, respectively. The higher frequency channel was tuned to the ¹²CO(4–3) line at 461.041 GHz in USB. We used the XFFTS backends providing a nominal 38 kHz spectral resolution for the 3–2 lines and 76 kHz for the 4–3 line. For each target, $90'' \times 90''$ on-the-fly (OTF) maps were obtained, using a relative reference off position $1000''$ away in right ascension. We started each observation by checking in total power mode whether the off positions are clean. If needed, we modified the OFF position ($1200''$ for V900 Mon and $800''$ for Bran 76), until we made sure that there is no CO emission at the velocity

¹ Konkoly Observatory, Research Centre for Astronomy and Earth Sciences, Hungarian Academy of Sciences, Konkoly-Thege Miklós út 15-17, 1121 Budapest, Hungary

² Max-Planck-Institut für Astronomie, Königstuhl 17, 69117 Heidelberg, Germany

³ Max-Planck-Institut für Radioastronomie, Auf dem Hügel 69, 53121 Bonn, Germany

Table 1
CO observations of our targets.

Name	Distance ^a (pc)	v_{LSR} (km s^{-1})	$F(^{12}\text{CO}(3-2))$ (Jy km s^{-1})	$F(^{12}\text{CO}(4-3))$ (Jy km s^{-1})	$F(^{13}\text{CO}(3-2))$ (Jy km s^{-1})	τ_{12}	τ_{13}	M_{tot} (M_{\odot})	Outflow?	Si feature
AR 6A/6B	800	5.3	3800±7	5190±39	1150±7	57	0.8	1.3 ^b	n	?
Bran 76	1700	17.7	18.8±1	21.4±5.7	4.27±1.39	24	0.4	0.02	n	em
HBC 494	460	4.3	3660±11	4780±50	1070±15	130	1.9	0.4	y	abs
HBC 687	400	17.2	173±6	164±22	37.0±6.7	15	0.2	0.01	n	em
Haro 5a IRS	470	11.2	7940±9	13800±50	2990±8	76	1.1	1.2	y	abs
OO Ser	311	8.1	15500±24	27800±140	3250±27	48	0.7	0.6	?	abs
V346 Nor	700	-3.0	2490±8	4780±33	383±8	52	0.8	0.3	y	abs
V900 Mon	1100	13.6	199±2	234±11	50.3±2.2	67	1.0	0.1 ^b	n	em

^a Distances are from Audard et al. (2014) and Reipurth & Aspin (1997).

^b For AR 6A/6B and V900 Mon, there is no distinct peak in the CO emission at the stellar position, therefore the CO emission (and masses given here) are most likely not associated with these sources.

of the target.

A first order baseline was removed from the spectra. The data were calibrated using a main beam efficiency of 0.73 and 0.60 at 352 and 464 GHz, respectively, and the values were converted to Jy using 41 Jy K^{-1} and 48 Jy K^{-1} at 352 and 464 GHz, respectively. The rms noise level calculated for the line-free channels in 1 km s^{-1} bins is 0.8 Jy for the $^{12}\text{CO}(3-2)$ and $^{13}\text{CO}(3-2)$ lines, and 2.3 Jy for the $^{12}\text{CO}(4-3)$ line. The telescope’s beam is $19''.2$, and $15''.3$ at the corresponding frequencies.

3. RESULTS AND ANALYSIS

CO emission for all targeted isotopologues and transitions were detected in our maps. In Fig. 1 we show the CO line profiles integrated within a 10000 au radius centered on the nominal position of our targets, while Fig. 2 shows the total CO line intensity maps integrated for the velocity channels where at least a 3σ signal was detected. The flux-weighted average v_{LSR} velocities for the CO emission are listed in Table 1. The velocity-integrated line fluxes for same spatial areas (within 10000 au) are also given in Table 1. We used the optically thin ^{13}CO lines to convert the observed line fluxes to total gas masses assuming local thermodynamic equilibrium, using 20 K temperature, a $^{13}\text{CO}/^{12}\text{CO}$ abundance ratio of 69 (Wilson 1999) and $^{12}\text{CO}/\text{H}_2$ abundance ratio of 10^{-4} (Bolatto et al. 2013). We note that if we use 50 K instead of 20 K , the masses would be a factor of 1.06 lower, and if we used 15 K instead of 20 K , the masses would be a factor of 1.29 times higher.

Line profiles— Figure 1 demonstrates that out of our sample, Bran 76 and HBC 687 show the narrowest lines, the FWHM is only about $0.7\text{--}0.8 \text{ km s}^{-1}$. V900 Mon is somewhat broader, while the rest of the targets show very broad lines, and prominent line wings in the ^{12}CO lines. For most of the sources (AR 6A/6B, HBC 494, Haro 5a IRS, V346 Nor, and V900 Mon), the ^{13}CO line is single-peaked, while the ^{12}CO lines are either flat-topped or show self-absorption. This suggests that ^{12}CO is optically thick. The same is true for the two targets with the narrow lines, where the ratio of the $^{12}\text{CO}(3-2)$ to the $^{13}\text{CO}(3-2)$ line peaks suggest a maximum optical depth of $\tau_{12}=15\text{--}24$ for the former and $\tau_{13}=0.2\text{--}0.4$ for the latter. For the rest of the targets, the line peaks indicate somewhat larger optical depths, in the $50\text{--}130$ range for τ_{12} and in the $0.7\text{--}1.9$ range for τ_{13} . The line profile of OO Ser is different from the other sources, because

even the ^{13}CO line seems to be double-peaked. Because the line ratios do not indicate extraordinarily high optical depths, we suspect that in this case several different velocity components are superimposed along the line of sight. The observed diversity of the line profiles seems to be a characteristic of the FUor class. Evans et al. (1994) presented single-dish CO line data for a sample containing both northern and southern FUors. In RNO 1B, V1735 Cyg, and V346 Nor they detected self-absorbed ^{12}CO , while Z CMa, V1057 Cyg, and V1515 Cyg displayed narrow, single-peaked ^{12}CO emission. The ^{13}CO line was single-peaked in all of their sources, similarly to our results.

Integrated emission maps— For all of our targets there is some CO emission towards the stellar position, but there is also significant confusion from extended emission. Bran 76, HBC 494, HBC 687, Haro 5a IRS, OO Ser, and V346 Nor, where the CO emission peaks at the stellar position, are clearly detected. For AR 6A/6B, and V900 Mon, the CO emission peak is offset, so it cannot be unambiguously associated with the star. In any case, the masses we calculated should be considered as upper limits for the envelope masses due to confusion. Three of our sources were targeted by Sandell & Weintraub (2001) in $850 \mu\text{m}$ and 1.3 mm continuum. While Bran 76 was undetected, for HBC 494 and V346 Nor they give envelope masses assuming 50 K for the dust temperature. Their values ($0.1 M_{\odot}$ for HBC 494 and $0.5 M_{\odot}$ for V346 Nor) are in good agreement with our mass estimates from the CO line fluxes using 50 K ($0.4 M_{\odot}$ for HBC 494 and $0.3 M_{\odot}$ for V346 Nor).

Comparison with dust continuum emission— In Fig. 1 we overplotted with contours the $250 \mu\text{m}$ emission using Herschel/SPIRE data from the Herschel Science Archive (proposal IDs: KPGT_fmotte_1, KPGT_pandre_1, OT1_maudar01_1). Herschel at this wavelength had a similar beam size ($18''$) to our APEX beam for the $J=3\text{--}2$ lines ($19''.2$). Generally there is a good agreement between the continuum and the CO line maps, although the continuum peaks are more prominent than the CO peaks, and there is less extended emission in continuum than in CO. Just like in CO, Bran 76, HBC 494, HBC 687, Haro 5a IRS, and V346 Nor are clearly detected in continuum, OO Ser is marginally detected, while AR 6A/6B seem to be sitting in the middle of a cavity. Unfortunately, V900 Mon was not observed by Herschel.

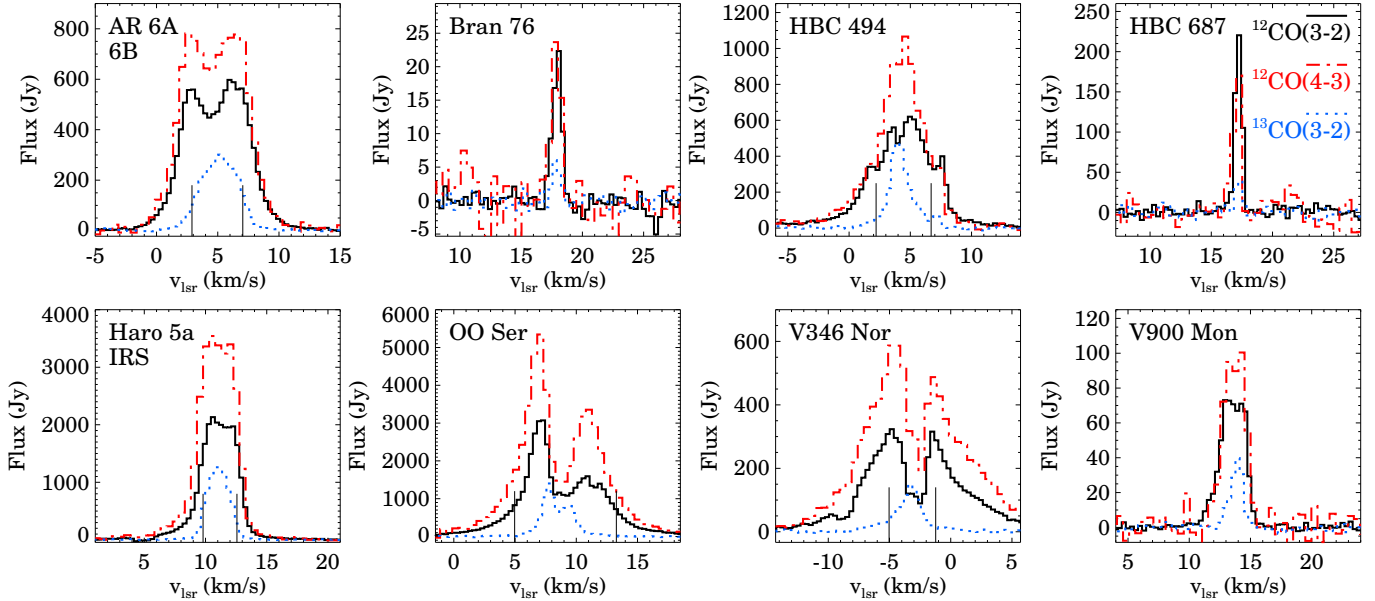


Figure 1. CO line profiles of our targets observed with APEX. Fluxes were integrated within a 10000 au radius centered on the nominal position of our targets. The line wings marked by the vertical lines indicate possible outflows.

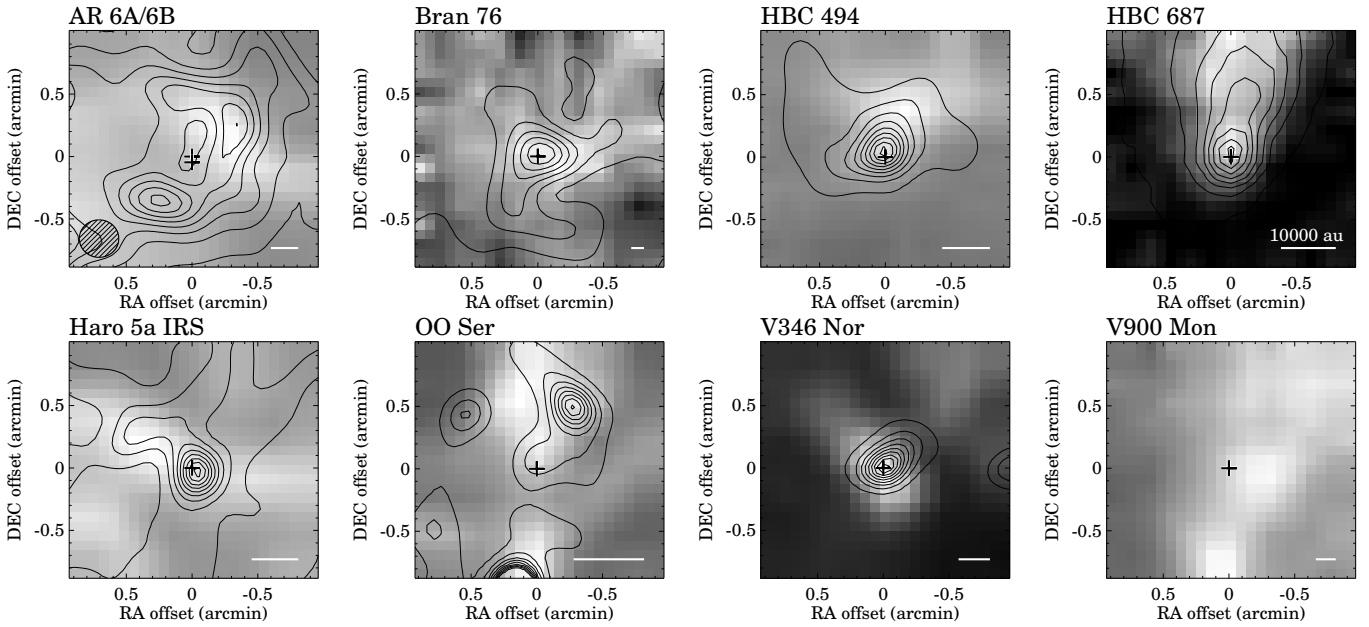


Figure 2. Integrated CO intensity maps of our targets for the $^{12}\text{CO}(3-2)$ line observed with APEX (grayscale) and $250\ \mu\text{m}$ continuum emission from Herschel (contours). Plus signs mark the stellar position, while the hatched circle shows the Herschel beam size.

Outflows— Some ^{12}CO lines have high-velocity wings, indicated by the vertical lines in Fig. 1. We integrated the emission for the red-shifted and blue-shifted parts and plotted the resulting maps with red and blue contours in Fig. 3. We detected clear signs for outflows in HBC 494, Haro 5a IRS, and V346 Nor. OO Ser may also drive an outflow, but at this spatial resolution, the detection is only tentative due to confusion in the area. For the three unambiguously detected outflows, we measured the masses, momenta, and energies of the blue and red lobes, following the method and equations presented in Dunham et al. (2014). The results, listed in Tab. 2, are calculated both in the optically thin approx-

imation, and by correcting for the optically thick emission using the $(1 - e^{-\tau_{12}})/\tau_{12}$ correction factor, where τ_{12} was calculated from the $^{12}\text{CO} / ^{13}\text{CO}$ line ratio in each velocity channel. The outflow masses, momenta, and energies of the FUors fall into the upper 30% compared to the distribution of these values measured by Dunham et al. (2014) for a sample of 28 outflows driven by low-mass protostars. The outflow of V346 Nor was already detected by Evans et al. (1994) in $^{12}\text{CO}(3-2)$ and by Reipurth et al. (1997) in the $^{12}\text{CO}(1-0)$, revealing a similar morphology of the outflowing gas as our data. Lee et al. (2002) observed HBC 494 in $^{12}\text{CO}(1-0)$. Their channel maps at $\approx 15''$ resolution look very similar to

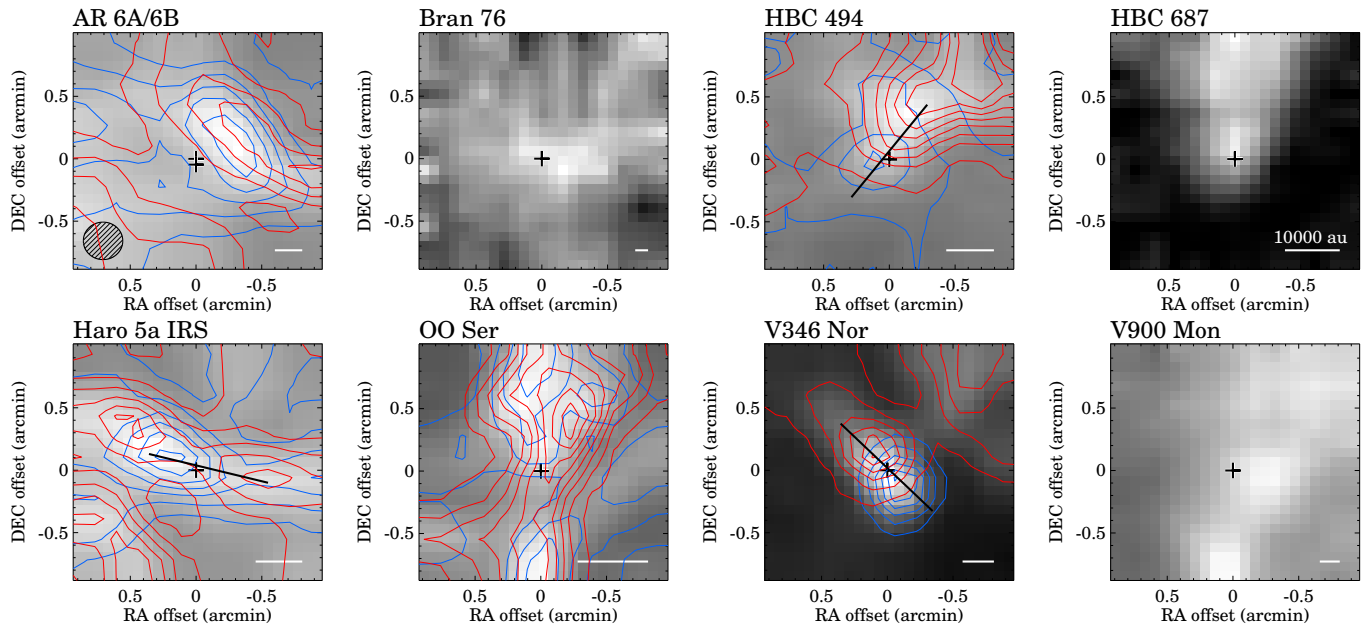


Figure 3. Integrated CO intensity maps of our targets for the $^{12}\text{CO}(3-2)$ line observed with APEX (grayscale). The red and blue contours show redshifted and blueshifted emission integrated in the velocity ranges indicated in Fig. 1 (contour levels are at 3, 6, 9, $\dots\sigma$). Thick black lines mark the directions of the detected bipolar outflows. Plus signs mark the stellar position, while the hatched circle shows the Herschel beam size.

ours. Haro 5a IRS and its surroundings were observed in $^{12}\text{CO}(1-0)$ and $^{12}\text{CO}(3-2)$ by Takahashi et al. (2006) and Takahashi et al. (2008). They clearly detected the CO outflow from Haro 5a IRS, and found an embedded protostellar candidate, MMS 7-NE, which also drives an outflow. This complex spatial and velocity structure of the CO emission is also reflected in our observations.

4. DISCUSSION AND CONCLUSIONS

Figure 1 and Table 1 reveal a striking variety of envelope properties within our sample. One of these properties is envelope mass. Haro 5a IRS, OO Ser, V346 Nor, and HBC 494 contain a significant amount of gas ($>0.3M_{\odot}$). HBC 678 and Bran 76 are associated with only 0.01-0.02 M_{\odot} of material. Having no associated CO peaks, AR 6A/6B and V900 Mon probably also have low-mass envelopes. Interestingly, other envelope parameters suggest an almost identical division of the sample. Envelopes with higher mass exhibit broader lines, while the low-mass envelopes have narrower lines or remain undetected towards the source. Temperatures calculated from the ratio of the $^{12}\text{CO}(4-3)$ and $^{12}\text{CO}(3-2)$ line ratios show that the low-mass envelopes are typically cold (5-7 K), while the higher-mass envelopes are warm (>40 K). Outflows are only detected from sources with higher-mass envelopes. By observing a large sample of low-mass protostars, Jørgensen et al. (2009) found that the envelope mass decreases sharply from typically $1M_{\odot}$ in Class 0 objects to $<0.1M_{\odot}$ in the Class I phase. Placing our targets into this evolutionary scheme, FUors with higher envelope masses represent a very early evolutionary phase. The FUors with low envelope masses or upper limits may be close to the end of the Class I phase.

As we summarized in the Introduction, Quanz et al. (2007) proposed a different way to order FUors into an evolutionary sequence: objects showing silicate absorption at $10\mu\text{m}$ are younger, still embedded in their opaque envelopes, while those showing silicate emission

are more evolved. We checked the Cornell Atlas of Spitzer/IRS Sources⁴ for mid-infrared spectra, and found that HBH 494, Haro 5a IRS, OO Ser, and V346 Nor have silicate absorption feature, while Bran 76, HBC 687, and V900 Mon exhibit emission (see also Tab. 1). Our division based on the CO gas properties of our targets correlates well with the division based on the $10\mu\text{m}$ silicate feature. Objects possessing massive gas envelopes exhibit silicate absorption, while those with lower-mass envelopes show silicate emission (Tab. 1). This conclusion suggests a parallel evolution of the circumstellar dust and gas in FUors.

When young stellar objects transition from the embedded to the disk-only phase, they clear away their envelopes to become an optically visible star. According to the hypothesis of Quanz et al. (2007), repetitive FUor outbursts may drive this process, since a thick obscuring envelope produces an absorption feature, while for an emission feature, large opening angle for the polar cavity in the envelope is needed to provide a clear line-of-sight to the inner disk (see also Kenyon & Hartmann 1991, Green et al. 2006). FUor outbursts gradually widen the outflow cavity due to the enhanced outflow activity during the eruptions.

During a typical FUor outburst $0.01M_{\odot}$ mass is accreted onto the central star (Hartmann 2008). Depending on the length of the quiescent periods, a similar amount of material may be accreted between the outbursts. This is comparable to the envelope mass found in our more evolved subsample. The mass reservoir in these systems to replenish the disk after an outburst is very small. Therefore, these objects are probably very close to the transition to the disk-only phase and may represent the links between the Class I and Class II phases of protostellar evolution.

⁴ <http://cassis.sirtf.com/>

Table 2
Outflow masses (M), momenta (P) and energies (E).

Parameter	HBC 494	Haro 5a IRS	V346 Nor
	optically thin		
M (blue) M_{\odot}	0.004	0.023	0.020
M (red) M_{\odot}	0.007	0.020	0.054
P (blue) $M_{\odot} \text{ km s}^{-1}$	0.016	0.039	0.076
P (red) $M_{\odot} \text{ km s}^{-1}$	0.017	0.042	0.228
E (blue) erg	7.8×10^{41}	8.2×10^{41}	3.8×10^{42}
E (red) erg	1.2×10^{42}	1.0×10^{42}	1.3×10^{43}
	optically thick		
M (blue) M_{\odot}	0.021	0.311	0.100
M (red) M_{\odot}	0.053	0.131	0.092
P (blue) $M_{\odot} \text{ km s}^{-1}$	0.061	0.417	0.281
P (red) $M_{\odot} \text{ km s}^{-1}$	0.166	0.244	0.312
E (blue) erg	2.1×10^{42}	6.2×10^{42}	9.3×10^{42}
E (red) erg	5.6×10^{42}	4.8×10^{42}	1.5×10^{43}

This work was supported by the Momentum grant of the MTA CSFK Lendület Disk Research Group, and the Hungarian Research Fund OTKA grant K101393. T.Cs. acknowledges support from the *Deutsche Forschungsgemeinschaft*, *DFG* via the SPP (priority programme) 1573 ‘Physics of the ISM’.

Facilities: APEX.

REFERENCES

Audard, M., Ábrahám, P., Dunham, M. M., et al. 2014, *Protostars and Planets VI*, 387

- Bell, K. R., & Lin, D. N. C. 1994, *ApJ*, 427, 987
 Bolatto, A. D., Wolfire, M., & Leroy, A. K. 2013, *ARA&A*, 51, 207
 Dunham, M. M., Arce, H. G., Mardones, D., et al. 2014, *ApJ*, 783, 29
 Evans, II, N. J., Balkum, S., Levreault, R. M., Hartmann, L., & Kenyon, S. 1994, *ApJ*, 424, 793
 Green, J. D., Hartmann, L., Calvet, N., et al. 2006, *ApJ*, 648, 1099
 Green, J. D., Evans, II, N. J., Kóspál, Á., et al. 2013, *ApJ*, 772, 117
 Güsten, R., Nyman, L. Å., Schilke, P., et al. 2006, *A&A*, 454, L13
 Hartmann, L. 2008, *Accretion Processes in Star Formation*
 Hartmann, L., & Kenyon, S. J. 1996, *ARA&A*, 34, 207
 Jørgensen, J. K., van Dishoeck, E. F., Visser, R., et al. 2009, *A&A*, 507, 861
 Kenyon, S. J., & Hartmann, L. W. 1991, *ApJ*, 383, 664
 Klein, T., Ciechanowicz, M., Leinz, C., et al. 2014, *IEEE Transactions on Terahertz Science and Technology*, 4, 588
 Lee, C.-F., Mundy, L. G., Stone, J. M., & Ostriker, E. C. 2002, *ApJ*, 576, 294
 McMurdoch, S., Sargent, A. I., & Blake, G. A. 1993, *AJ*, 106, 2477
 Quanz, S. P., Henning, T., Bouwman, J., et al. 2007, *ApJ*, 668, 359
 Reipurth, B., & Aspin, C. 1997, *AJ*, 114, 2700
 Reipurth, B., Olberg, M., Gredel, R., & Booth, R. S. 1997, *A&A*, 327, 1164
 Sandell, G., & Weintraub, D. A. 2001, *ApJS*, 134, 115
 Takahashi, S., Saito, M., Ohashi, N., et al. 2008, *ApJ*, 688, 344
 Takahashi, S., Saito, M., Takakuwa, S., & Kawabe, R. 2006, *ApJ*, 651, 933
 Vorobyov, E. I., & Basu, S. 2006, *ApJ*, 650, 956
 Wilson, T. L. 1999, *Reports on Progress in Physics*, 62, 143